J Therm Anal Calorim (2011) 103:845–851
DOI 10.1007/s10973-010-1192-z

# Kinetics and dissociation mechanism of heptaaqua-*p*-nitrophenolatostrontium(II) nitrophenol

**Jeya Rajendran · T. Lekshmana Thanu Lingam · M. Jose · S. Jerome Das**

Received: 8 August 2010 / Accepted: 15 November 2010 / Published online: 15 December 2010


**Abstract** A single crystal of heptaaqua-*p*-nitrophenolatostrontium(II) nitrophenol (HNSN) was grown, and the structure was confirmed by UV–Vis–NIR, FT-IR, FT-NMR, and high-resolution X-ray diffraction (HRXRD) analyses. The dielectric loss, dielectric constant, and the mechanical strength of the crystal have already been reported. The dynamic, non-isothermal thermal analysis was carried out at different heating rates, and TG and DTG data were used for the interpretation of the mechanisms and kinetics of decomposition by means of a model fitting method, Coats–Redfern equation, and a model-free method, Kissinger and Flynn–Wall method. The values of activation energy ($E$) and the pre-exponential factor (ln $A$) of each stage of thermal decomposition at various linear heating rates were calculated.

**Keywords** Energy of activation · Heptaaqua-*p*-nitrophenolatostrontium(II) nitrophenol · Kinetics · Thermal analysis

J. Rajendran (✉)
Department of Chemistry, Loyola College, Nungambakkam, Chennai, Tamilnadu 600 034, India
e-mail: jeyarajendran@yahoo.com

T. Lekshmana Thanu Lingam
Fireworks Research and Development Centre, Petroleum and Explosives Safety Organisation, Anayoor Village, Sivakasi, Tamilnadu 626 124, India

M. Jose · S. Jerome Das
Department of Physics, Loyola College, Nungambakkam, Chennai, Tamilnadu 600 034, India

## Introduction

Crystals with high hyper polarizability result in larger values of second-order non-linear susceptibilities that have great potential in the applications of constructing molecular devices such as frequency converters, electro optic switching, etc. [1]. The lifetime of a crystal can be understood with the knowledge of mechanical and thermal stability of the crystal. Moreover, improvements of crystal quality also depend on knowing the thermo dynamical properties and thermal stabilities of the crystals and the information are needed to avoid unwanted structural changes during storage and formulation. The choice of crystalline phase depends upon its thermodynamic stability and physical properties such as hygroscopicity, solubility, and thermal stability. The most stable crystalline phase, by definition, has the lowest thermodynamic stability. The single crystalline nature of the sample is the most ordered form of the sample and degradation of the sample brings disorder in the sample [2].

Single crystal of heptaaqua-*p*-nitrophenolatostrontium(II) nitrophenol (HNSN) was grown with dimension $40 \times 12 \times 6$ mm$^3$ using slow evaporation solution growth technique at constant temperature (313 K) and was characterized [3]. In this study, thermal stability studies were carried out. Dissociation mechanism and kinetic parameters were done by employing physical model-dependent methods [4, 5] and model-free methods [6–9].

## Experimental

### Synthesis and characterization

The complex HNSN was synthesized from paranitrophenol and strontium hydroxide (octahydrate) in the

stoichiometric ratio 1:1. The complex was recrystallized using water as solvent. The purified compound was stirred continuously resulting in a homogenous solution which was then kept undisturbed at a constant temperature of 313 K. A single crystal of the complex, HNSN of dimension $40 \times 12 \times 6$ mm$^3$ was isolated from the supersaturated solution. The structure of the complex was characterized by UV–Vis–NIR, FT-IR, NMR, and XRD analyses. UV–Vis spectral analysis was carried out using Varian Cary 5E in the range 200–2,000 nm. FT-IR spectrum was recorded using Bruker IFS 66v FT-IR spectrometer. $^1$H NMR spectrum of the complex was recorded by a Bruker Advance III 500 MHz FTNMR using $D_2O$ as solvent. X-ray data of the compound HNSN were collected at room temperature using a Bruker Smart Apex CCD diffractometer with graphite monochromated MoK, radiation ($\lambda = 0.71073$ Å) with $\omega$-scan method. Molecular graphics were computed using DIAMOND program [10]. The conventional, non-isothermal, thermo gravimetric (TG), differential thermogravimetric (DTG), and differential thermal analysis (DTA) were carried out using a Perkin-Elmer diamond model thermal analyzer with different heating rates 1, 3, and 5 K/min ranging from room temperature to 1,173 K using nitrogen gas atmosphere. Model-free methods, Arrhenius, Kissinger, and Flynn–wall methods and model fitting methods, Coats–Redfern, were followed among the several methods available for the kinetics evaluation of TG mass loss data.

HNSN was characterized by UV, IR, NMR, and XRD analyses. The crystal was found to be transparent between 500 and 2,000 nm (visible and near infrared region). FT-IR spectrum was recorded between 450 and 4,000 cm$^{-1}$ with the characteristic peaks (3,434 cm$^{-1}$ for $\gamma_{OH}$ stretching, 1,648 cm$^{-1}$ for $\gamma_{H_2O}$ bending, 1,312 cm$^{-1}$ for $\gamma_{NO_2}$ stretching, 1,811 cm$^{-1}$ for 1,4 disubstituted phenyl ring, and 819 cm$^{-1}$ for $\gamma_{CN}$ vibration) [11].

Three non-overlapping peaks of FTNMR spectra in which doublet (at $\delta = 6.269$ and 6.250 ppm, $J = 9.5$ Hz) corresponds to deshielded hydrogen adjacent to $NO_2$ group, doublet (at $\delta = 4.742$ and 4.723 ppm, $J = 9.5$ Hz) corresponds to hydrogen adjacent to OH group, and a singlet (at $\delta = 3.037$ ppm) corresponds to $H_2O$ were assigned.

The structure was solved by direct methods using SHELXS97 and refinement was carried out by full-matrix least-squares technique using SHELXL97 [12]. Molecular graphics were computed [3] using DIAMOND [10] program at 30% probability level.

## Thermal properties of $[Sr(C_6H_4NO_3)(H_2O)_7]C_6H_4NO_3$

The rates and other kinetic parameters of thermal decomposition of compounds depend largely upon their structures. The conventional, non-isothermal, thermograms (TG and DTG) for HNSN, at three different heating rates, 1, 3, and 5 K/min are shown in Figs. 1 and 2, respectively. Increase in heating rate leads to an increase in the characteristic peak temperature ($T_p$) which can be seen in the thermograms (Figs. 1, 2). Decomposition occurred only by two stages by increasing the heating rate also. In DTG (Fig. 2), first step of decomposition is not seen clearly due to the prominent peak of the second stage which is discussed at the end of this article. The first mass loss occurred between 298 and 423 K which corresponds to the loss of seven molecules of water of crystallization and appears as an endothermic peak in the DTA curve (Fig. 3). There is a good agreement between the expected and

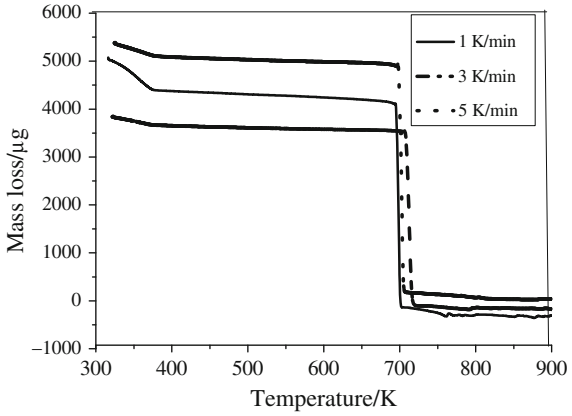


**Fig. 1** TG curves of HNSN in nitrogen atmosphere; heating rate of 1, 3, and 5 K/min

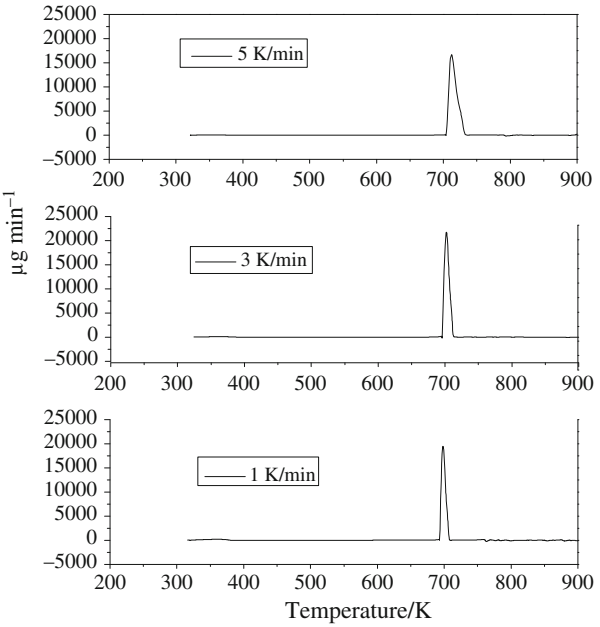


**Fig. 2** DTG curves in nitrogen atmosphere; heating rate of 1, 3, and 5 K/min

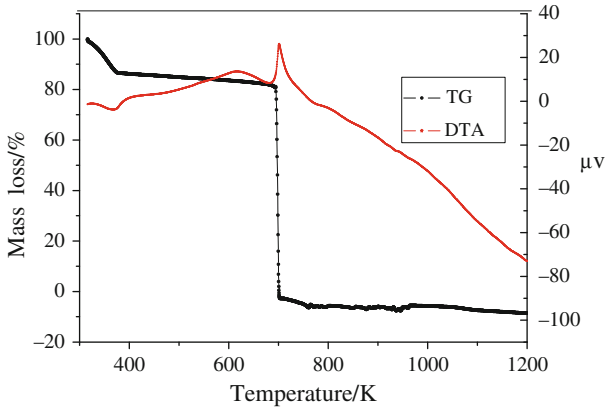


**Fig. 3** TG and DTA curves of HNSN in nitrogen atmosphere; heating rate: 1 K/min

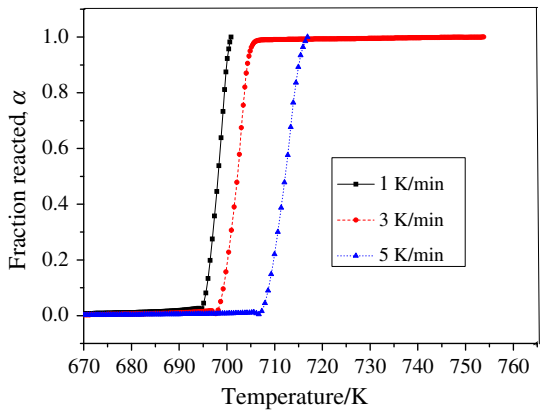


**Fig. 4** Fraction reacted, α versus temperature for stage II at three different heating rates

observed mass loss for the loss of seven moles of water as shown in Table 1. The sharp mass loss at 700 K is assigned to the degradation of paranitrophenolate group into fragments and the subsequent volatilization. Two-stage decompositions indicated the difference in the strength of the bond, between water and nitrophenolic group attaching with metal, which are proved by XRD analysis.

The kinetics of the thermal decomposition of HNSN at different heating rates was studied by model-dependent and model-free methods.

## Determination of energy of activation, $E_a$—model-free methods

The transformation rate during a reaction is the product of two functions, one depending solely on the temperature, $T$, and the other depending solely on the fraction transformed, α:

$$d\alpha/dt = f(\alpha)k(T) \quad (1)$$

where $d\alpha/dt$ is the derivative of the fraction converted with respect to time and it was calculated for every 10% mass loss of the complex for both stage of decomposition in the temperature range 313–381 and 673–713 K at different heating rates. α is defined by the expression as

$$\alpha = (\%w_i - \%w_t)/(\%w_i - \%w_f) \quad (2)$$

where $\%w_t$ is the mass percent at any time $t$ and $\%w_i$ and $\%w_f$ are the initial and final mass percent sample [13], respectively. A typical plot of α versus temperature for

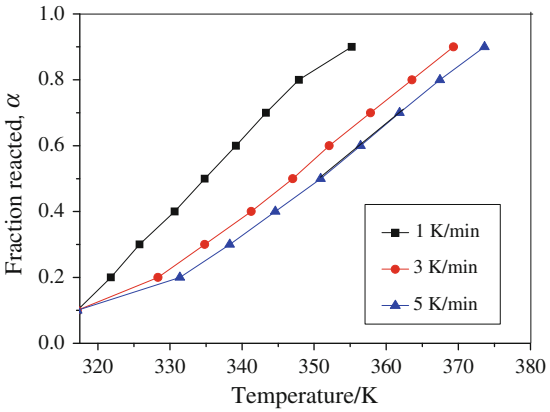


**Fig. 5** Fraction reacted, α versus temperature for stage I at three different heating rates

stages I and II is shown in Figs. 4 and 5. The temperature-dependent function is generally assumed to follow an Arrhenius type dependency

$$\ln k = \ln A - E_a/RT \quad (3)$$

Thus, to describe the progress of the reaction at all temperatures and for all temperature–time programmes, the function $f(\alpha)$, and the constants ln $A$ and $E$ need to be determined. For non-isothermal experiments, the reaction rate at all times depends on both $f(\alpha)$ and $k(T)$, and hence on the determination of $f(\alpha)$, ln $A$ and $E$ (the so-called kinetic triplet). The linear Arrhenius plots of ln $k$ versus

**Table 1** Comparison of the expected and observed mass loss for the decomposition of HNSN at 3 K/min in nitrogen atmosphere

| Assumed reactions | Temperature/K | Cumulative mass loss/% | |
|---|---|---|---|
| | | Expected | Observed |
| $[Sr(C_6H_4NO_3)(H_2O)_7]\ C_6H_4NO_3 \rightarrow [Sr(C_6H_4NO_3)]\ C_6H_4NO_3 + 7H_2O$ | 381 | 25.71 | 25.83 |
| $[Sr(C_6H_4NO_3)]\ C_6H_4NO_3 \rightarrow$ volatile oxides | 700 | 74.29 | 74.17 |

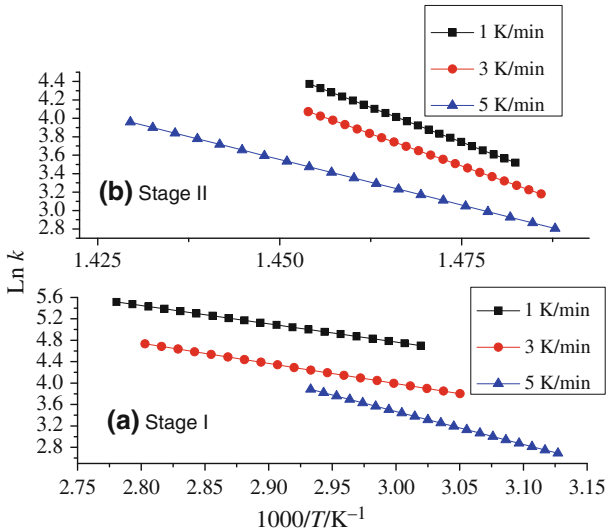


**Fig. 6** Arrhenius plot of ln $k$ versus temperature for non-isothermal decomposition of HNSN in nitrogen atmosphere for **a** stage I and **b** stage II

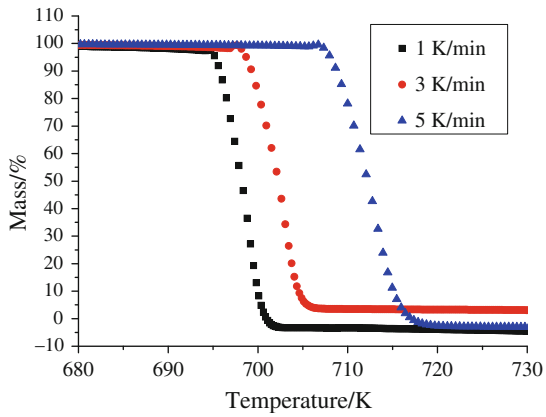


**Fig. 7** Mass loss (%) versus temperature for stage I decomposition of HNSN at three different heating rates

$1/T$ for the two stage decompositions of HNSN at various heating rates were plotted (Fig. 6a, b) from the non-isothermal DTG data. From the slope, the activation energy ($E_a$) for the decomposition of the complex was calculated (Table 2). The activation energy values obtained are 28 ± 3.4, 31 ± 4.2, 39 ± 4.6 kJ mol$^{-1}$ for stage I, and 101 ± 6.3, 96 ± 4.5, 72 ± 3.9 kJ mol$^{-1}$ for stage II, respectively.

The activation energy for the non-isothermal decomposition of the complex HNSN was calculated from the TG data (Fig. 7 for stage II and similar plot for stage I is also obtained) using Kissinger expression:

$$\ln\left(\beta/T_m^2\right) = \ln(n(1-\alpha_m)^{n-1}AR/E_a) - E_a/RT \quad (4)$$

where $\beta$ is the heating rate, $A$ is the pre-exponential factor, $E_a$ is the energy of activation, $T_m$ and $\alpha_m$ are the absolute temperature and mass loss at the maximum mass loss rate $(d\alpha/dt)_m$, and $R$ is gas constant. This method yielded a value of 33 ± 2.0 and 85 ± 2.0 kJ mol$^{-1}$ for stage I and II, respectively (Table 2) from the slope of $ln\ (\beta/T_m^2)$ as a function of $1/T_m$ at the maximum mass loss rate.

The fraction reacted $\alpha$, range of 0.10–0.8 and 0.10–0.9 were used for the kinetic analysis of the first and second stages, respectively. The activation energy for each conversion point ($E_a$, $\alpha$) was calculated using Flynn–Wall method at different heating rate, $\beta$ using the expression,

$$\ln\beta = \ln(AE_a/R) - \ln[F(\alpha)] - E_a/RT \quad (5)$$

The decomposition of the complex was carried out at different heating rates ($\beta$) in this technique. The plot of the different heating rates against the temperature at every heating rate is shown in Figs. 8 and 9, and the straight lines obtained are nearly parallel to each other showing the

**Table 2** Kinetic parameters of non-isothermal decomposition of HNSN by various techniques

| $\beta$ | Arrhenius | | Kissinger | | Flynn–Wall | | | | | |
|---|---|---|---|---|---|---|---|---|---|---|
| | | | | | Stage I | | | Stage II | | |
| | $E_a$ | ln A | $E_a$ | ln A | $\alpha$ | $E_a$ | ln A | $\alpha$ | $E_a$ | ln A |
| Stage I | | | | | 0.1 | 27.802 | 2.649 | 0.1 | 97.194 | 20.069 |
| 1 | 28.342 | 14.994 | 33.33 | 2.994 | 0.2 | 27.427 | 2.499 | 0.2 | 94.70 | 19.626 |
| 3 | 31.245 | 15.284 | 85.55 | 17.988 | 0.3 | 22.994 | 2.309 | 0.3 | 92.70 | 19.255 |
| 5 | 39.49 | 20.558 | | | 0.4 | 17.17 | 2.114 | 0.4 | 92.82 | 19.261 |
| Stage II | | | | | 0.5 | 14.780 | 2.098 | 0.5 | 92.86 | 19.263 |
| 1 | 101.43 | 18.55 | | | 0.6 | 13.493 | 1.992 | 0.6 | 92.86 | 19.263 |
| 3 | 96.192 | 17.52 | | | 0.7 | 12.712 | 1.609 | 0.7 | 90.21 | 18.789 |
| 5 | 72.332 | 13.10 | | | 0.8 | 12.595 | 1.558 | 0.8 | 87.479 | 18.299 |
| | | | | | 0.9 | – | – | 0.9 | 85.557 | 17.969 |

$\beta$ heating rate, $\alpha$ fraction converted

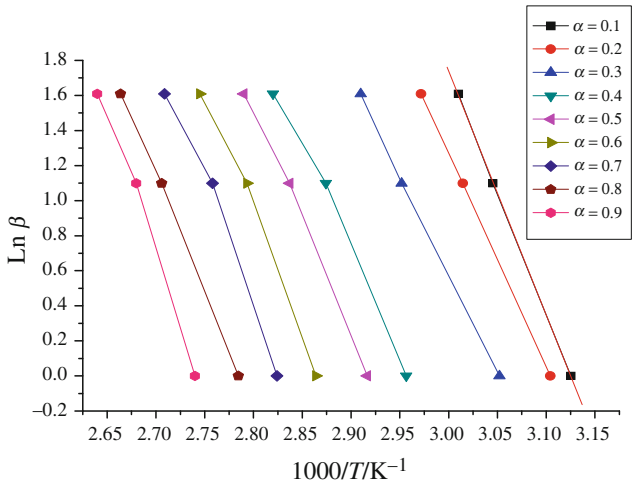


**Fig. 8** Flynn–Wall plot for stage I in nitrogen atmosphere for the non-isothermal decomposition of HNSN using TG data

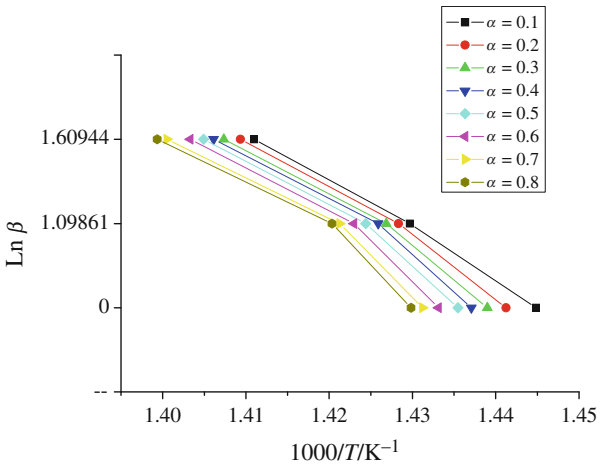


**Fig. 9** Flynn–Wall plot for stage II in nitrogen atmosphere for the non-isothermal decomposition of HNSN using TG data

applicability of this method to metal–organic complexes. The mean activation energy of 18 ± 4 and 91 ± 4 kJ $mol^{-1}$ for stages I and II was found for the mass loss range 10–80%, and this value was found to be comparable with the result of Kissinger method.

The non-isothermal, TG experimental data were also used to study the apparent activation energy, $E_a$ as a function of the extent of conversion, α. The activation energy for each conversion point ($E_a$, α) was calculated from the slope of the linear plot of Flynn–Wall method at different heating rate, β. The plot, $E_a$ versus α, fraction reacted for stage I (Fig. 10a) shows that $E_a$ decreases with the extent of conversion (α), $0.1 < \alpha < 0.9$ except at $\alpha = 0.6$, whereas three different regions exist in the decomposition of stage II (Fig. 10b). That the activation energy is high at the initial fraction reacted indicates that the decomposed products are in equilibrium with the

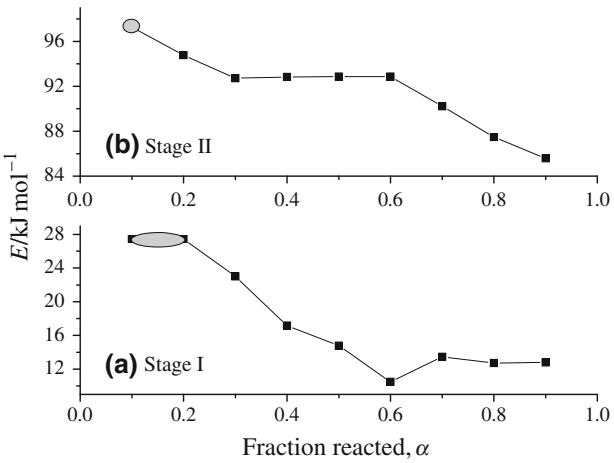


**Fig. 10** Dependence of the apparent value of $E$ versus α, fraction reacted by Flynn–Wall method for **a** stage I and **b** stage II

gaseous reactants. The results revealed that the dependence of the apparent activation energy ($E_a$) on the extent of conversion helps not only to disclose the complexity of a decomposition process, but to identify its kinetic scheme as well. The $E$ value is lower for stage I (27.444 kJ $mol^{-1}$) indicating that the rate of decomposition is fast compared to the second stage (97.2555 kJ $mol^{-1}$). In stage II, the conversion range, $0.3 < \alpha < 0.6$, the apparent activation energy is approximately independent of the extent of conversion, which is indicative of the irreversible process and more than one mechanism operates during the decomposition process of compound.

## Dissociation mechanism/model fitting method

Kinetic analysis by model fitting methods [14–16] was carried out to predict the mechanism of dissociation processes and to deduce the kinetic parameters. Kinetic analysis of thermoanalytical data where there is a linear temperature rise (β) has most often been based on the rate equation

$$\beta \mathrm{d}\alpha/\mathrm{d}t = A\exp^{(-E/RT)} f(\alpha) \quad (6)$$

which states that the rate of the reaction is proportional to the rate coefficient with Arrhenius temperature dependence and a function of the degree of conversion, $f$(a). Concentration of a solid is not usually a meaningful term for solid-state reactions. Equation 6 can be represented by its integral form as follows:

$$\ln\left[g(\alpha)/T^2\right] = \ln[(AR/\beta E)(1 - 2RT/E)] - -E/RT \quad (7)$$

where, $A$ is the pre-exponential factor, $E$ the activation energy and $R$ is the gas constant. The algebraic expression of the integral $g(\alpha)$ functions for P1, E1, A2, A3, A4, B1, R2, R3, D1, D2, D3, and D4 model mechanisms are tested

**Table 3** Kinetic parameters and possible rate controlling processes of decomposition of HNSN

| Mech | $\beta$/K/min | TG data | | Correlation coefficient ($r$) |
|---|---|---|---|---|
| | | $E$/kJ mol$^{-1}$ | ln $A$/min | |
| Stage I | | | | |
| A2 | 1 | 26.588 | 1.0799 | 0.9983 |
| | 3 | 43.448 | 1.8949 | 0.9942 |
| | 5 | 30.198 | 3.1723 | 0.9958 |
| Stage II | | | | |
| A3 | 1 | 172.29 | 14.9567 | 0.9995 |
| | 3 | 140.34 | 12.5808 | 0.9992 |
| | 5 | 102.59 | 11.8012 | 0.9845 |

in this study [4, 5]. A plot of ln $g(\alpha)/T^2$ versus $1/T$ gives a straight line when the correct $g(\alpha)$ function is used in the equation. The $g(\alpha)$ function describes the mechanism of the reaction. Straight lines with high-correlation coefficient and low standard deviation were selected to represent the possible controlling mechanism.

The kinetics of the two stages of the thermal decomposition of HNSN was followed by employing the Coats–Redfern approximation [4, 5]. Model fitting is performed by linear fit method in the conversion region where the apparent activation energy is approximately constant. The non-isothermal kinetic data of compound in the limit of $0.1 < \alpha < 0.9$ are fitted to each of the thirteen reaction model. The values of activation energy ($E_a$), pre-exponential factor (ln $A$) and the coefficient of linear correlation ($r$) for various kinetic models at three different heating rates are presented in Table 3. The Arrhenius parameters ($E_a$, ln $A$) of decomposition are highly variable, exhibiting a strong dependence on the reaction model chosen. On the other hand, more than one model, namely, R2 and A2 for stage I, and D3 and A3 for stage II gave fairly good

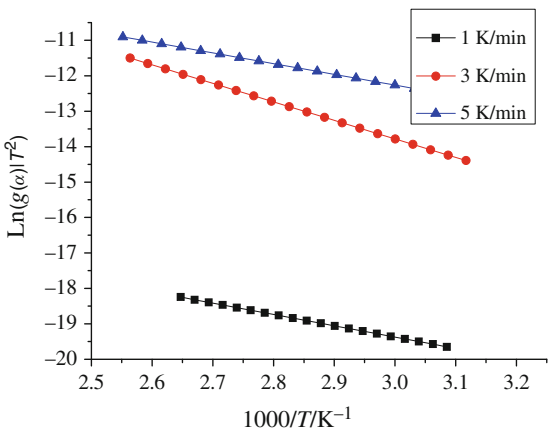


**Fig. 11** Plot of $[g(\alpha/T^2)]$ versus $1/T$ for stage I using TG data, $g(\alpha) = -\ln(1-\alpha)^{1/2}$

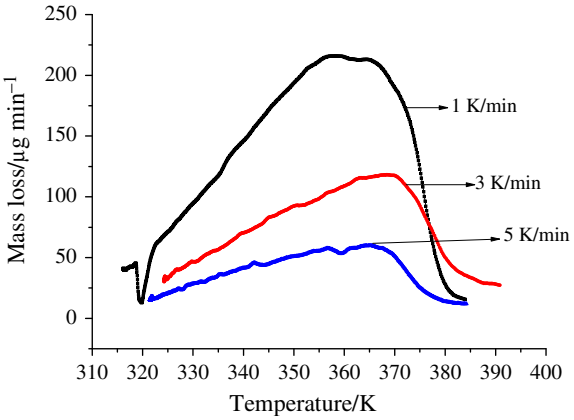


**Fig. 12** DTG curves of stage I in nitrogen atmosphere; heating rates of 1, 3, and 5 K/min

coefficient of linear equation lines. However, by comparing the $E_a$ value with the model-free method, A2, two-dimensional Avrami–Erofe'ev model (Fig. 11) which corresponds to nucleation and growth mechanism and A3 mechanism, Avrami–Erofe'ev random nucleation, 3D growth were accepted for stages I and II, respectively [15]. The activation energy obtained for the second step was found to be much higher than the values obtained for the dehydration step. Theoretically the activation energy of a process is expected not to change with change in heating rate. But the activation energy of stage I is found to increase with the heating rate of 1–3 K/min and decrease from 3 to 5 K/min and there is direct correlation with the peak temperature of the corresponding DTG plot of stage I (Fig. 12) and the activation energy for stage II is found to decrease with increase in heating rate and this has been reported in the literature [14]. Similarly pre-exponential factor was also found to change with heating rate. The real activation energy for each decomposition step would be the one obtained under lowest heating rate.

## Conclusions

The thermal decomposition of the complex HNSN $[Sr(C_6H_4NO_3)(H_2O)_7]C_6H_4NO_3$ occurs in two steps. The first stage of dehydration occurs at 313–383 K and the second stage of decomposition of dehydrated complex $[Sr(C_6H_4NO_3]C_6H_4NO_3$ occurs at 674–745 K. The dehydration is governed by A2 and the decomposition is governed by A3 mechanism. Kinetic parameters were deduced at each stage under non-isothermal conditions by model-free and model fitting methods and the values are comparable.

**Acknowledgements** The authors thank Kitheri Joseph, Scientific officer, Indira Gandhi Center for Atomic Research, Kalpakkam, for her fruitful suggestions.

## References


1. Dmitriev VG, Gurzadyan GG, Nicogosyan DN. Handbook of nonlinear optical crystals. New York: Springer Verlag; 1999.
2. Oana Carp RD, Budrugeac P, Niculescu M, Segal E. Nonisothermal decomposition kinetics of $[CoC_2O_4{\cdot}2.5H_2O]n$. J Therm Anal Calorim. 2010;:1–6. doi:10.1007/s10973-010-1037-9.
3. Jose M, Sridhar B, Bhavannarayana G, Sugandhi K, Uthrakumar R, Justin Raj C, Tamilvendhan D, Das SJ. Growth, structural, optical, thermal and mechanical studies of novel semi-organic NLO active single crystal: heptaaqua-*p*-nitrophenolato strontium (I) nitrophenol. J Cryst Growth. 2010;312:793–9.
4. Coats AW, Redfern JP. Kinetic parameters from thermo gravimetric data. Nature. 1964;201:68–9.
5. Coats AW, Redfern JP. Kinetic parameters from thermogravimetric data, II. Polym Lett. 1965;3:917–20.
6. Kissinger HE. Reaction kinetics in differential thermal analysis. Anal Chem. 1957;27:1702–6.
7. Kissinger HE. Variation of peak temperature with heating rate in differential thermal analysis. J Res Natl Bur Stand. 1956;57:217–21.
8. Ozawa T. Non-isothermal kinetics and generalized time. Thermochim Acta. 1986;100:109–18.
9. Flynn JH, Wall LA. A quick, direct method for the determination of activation energy from thermogravimetric data. J Polym Sci B Polym Lett. 1966;4:323–8.
10. Brandenburg K, Putz H. DIAMOND. Release 3.0c. Bonn: Crystal Impact GbR; 2005.
11. Nakamoto K. Infrared and Raman spectra of inorganic and coordination compounds. 3rd ed. New York: John Wiley; 1978.
12. Su TT, Zhai YC, Jiang EH, Gong M. Studies on the thermal decomposition kinetics and mechanism of ammonium niobium oxalate. J Therm Anal Calorim. 2009;98:449–55.
13. Papadopoulos C, Kantiranis N, Vecchio S, Lalia MK. Lanthanide complexes of 3-methoxy-salicylaldehyde. Thermal and kinetic investigation by simultaneous TG/DTG–DTA coupled with MS. J Therm Anal Calorim. 2010;99:931–8.
14. Joseph K, Sridharan R, Gnanasekaran T. Kinetics of thermal decomposition of $Th(C_2O_4)_2{\cdot}6H_2O$ [J]. J Nucl Mater. 2000;281:129–39.
15. Starink M. The determination of activation energy from linear heating rate experiments: a comparison of the accuracy of isoconversion methods. J Thermochim Acta. 2003;404(1):163–76.
16. Zhang JJ, Wang RF, Li JB, Liu HM. Thermal decomposition of (4,4-dimethyl-2,2-bipyridine) tris(benzoate) europium(III) non-isothermal kinetics. J Therm Anal Calorim. 2001;65:241–8.